

A Position Controller for Hydraulic Excavators With Deadtime and Regenerative Pipelines

Yuki Yamamoto^{ID}, Jinjun Qiu, Takayuki Doi, Takao Nanjo, Koji Yamashita, and Ryo Kikuuwe^{ID}, *Member, IEEE*

Abstract—This paper proposes a position controller for commercial hydraulic excavators. It is constructed by combining a proportional-derivative (PD) controller and a sliding-mode controller as a differential algebraic inclusion and also is integrated with a recently-proposed hydraulic actuator model. The use of the PD control is intended to make the controller insensitive to the deadtime in the hydraulic system, which is typically 0.1 s to 0.6 s in commercial excavators. The use of the sliding-mode controller combined with the actuator model is for handling the saturation of the actuator force, which may happen when the target position is not close enough to the current position and when the relief valves open. Moreover, this paper extends the controller to deal with the effect of the regenerative pipelines, which are embedded in commercial excavators to realize efficient operations but act as a source of disturbance on the controller. This paper also shows an analysis that can be used for tuning the controller parameters. The proposed controller was validated with simulations and experiments using a 13-ton class excavator, in which some set-point control tasks and trajectory-tracking tasks were performed.

Note to Practitioners—This paper proposes a position controller for hydraulic excavators. The controller was validated with the boom and arm actuators of a 13-ton class commercial excavator, with trajectory-tracking and set-point control tasks. Most of the controller parameters can be set referring to available specifications of the hydraulic circuit, such as the set pressures of the relief valves and the cross-sectional areas of the chambers. There are three parameters (the proportional gain, the derivative gain, and the time constant of the convergence) that should be carefully tuned, but their physical interpretations are relatively straightforward, and they can also be tuned along our guideline using pole locations of a particular transfer function. It has been shown that the proposed controller properly works despite the existence of the deadtime in the hydraulic systems, which are typically 0.1 s to 0.6 s. An extended version of the proposed controller handles the effects of the regenerative pipeline, which exists in some hydraulic systems, e.g., the arm actuator, for efficient operation and is not accounted for in the original version

of the controller. The accuracy of the proposed controller will be further improved by combining it with better means to estimate external forces by using additional sensors, such as pressure sensors installed to actuator chambers.

Index Terms—Position control, hydraulic systems, time delay.

I. INTRODUCTION

POSITION control technology for hydraulic excavators is a prerequisite for future automation in construction sites. The actuators used in commercial excavators are composed of many valves and pipelines, which cause strong nonlinearity in the response characteristics of the actuators. Specifically, the check valves and the relief valves in the hydraulic circuit act as on-off switches of the oil flow, and thus result in non-differentiability or discontinuity in the velocity-force and flowrate-pressure relations. Such features of hydraulic systems pose difficulty in the control of excavators.

One approach for the control of hydraulic systems is employing a locally linearized model of the system. Some controllers [1], [2], [3], [4] with linearized models are reported to achieve tracking tasks with smooth position commands. Another approach is combining gain-tuning methods with linear controllers [5], [6], [7], [8] in which the control gains are optimized in metaheuristic algorithms. Some researchers [9], [10], [11], [12], [13] employ neural networks to approximate the actuator characteristics, but the actuator force saturation, which frequently happens and discontinuously alters the response characteristics, has not been taken into account.

Another problematic factor in the control of hydraulic systems is the deadtime, which is typically 0.1 s to 0.6 s or more [2], [4], [14] in commercial hydraulic excavators. There have been some controllers based on models of the deadtime in hydraulic systems [2], [4], [11], [12], but they require the identification of the deadtime, and the control performance depends on the precision of the identification.

Recently, the authors proposed a set-point position controller [14] for hydraulic excavators. It analytically considers the circuit structure, composed of various valves and pipelines, by employing a quasistatic actuator model [15]. It can be seen as a particular type of a sliding-mode controller combined with a deadtime compensation based on the dynamics model of the excavator. Its biggest problem is that its control performance highly depends on the accuracy of the state prediction, employing the plant dynamics model, for the deadtime compensation.

Manuscript received 12 September 2023; revised 21 November 2023; accepted 31 December 2023. This article was recommended for publication by Associate Editor L. Bascetta and Editor B. Vogel-Heuser upon evaluation of the reviewers' comments. This work was supported by Kobelco Construction Machinery Company Ltd. (Corresponding author: Yuki Yamamoto.)

Yuki Yamamoto is with the Machinery Dynamics Laboratory, Hiroshima University, Higashihiroshima, Hiroshima 739-8527, Japan, and also with the Japan Society for the Promotion of Science, Tokyo 102-0083, Japan (e-mail: y.yamamoto@mdl.hiroshima-u.ac.jp).

Jinjun Qiu, Takayuki Doi, Takao Nanjo, and Koji Yamashita are with Kobelco Construction Machinery Company Ltd., Hiroshima 731-5161, Japan.

Ryo Kikuuwe is with the Machinery Dynamics Laboratory, Hiroshima University, Higashihiroshima, Hiroshima 739-8527, Japan.

Color versions of one or more figures in this article are available at <https://doi.org/10.1109/TASE.2024.3354952>.

Digital Object Identifier 10.1109/TASE.2024.3354952

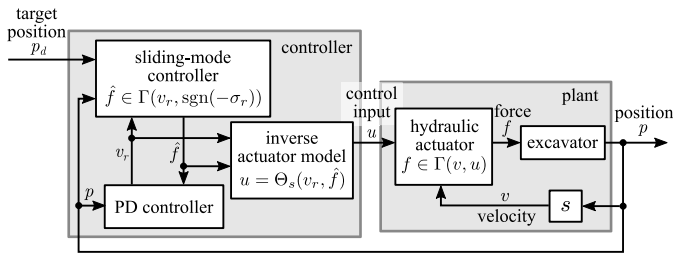


Fig. 1. Block diagram of the proposed controller, where v_r is a reference velocity, \hat{f} is the intended actuator force, and u is the control input to determine the opening ratios of the main control valves. The functions Γ and Θ describe the quasistatic relation among the force f , the velocity v , and the control input u , as detailed in Section II-C. The sliding surface is $\sigma_r \triangleq p - p_d + H(v_r - \dot{p}_d) = 0$.

This paper proposes yet another position controller for hydraulic actuators that is also a sliding-mode-like controller but is free from explicit compensation for the deadline. The motivation for the controller design is to avoid using a priori knowledge of the plant dynamics and the deadline, which is usually difficult to obtain in real-world applications. The controller has a structure illustrated in Fig. 1. It is a differential-algebraic combination of a sliding-mode controller and a proportional-derivative (PD) controller, and employs the quasistatic actuator model [15] to determine the control input. The use of the PD controller is to realize a certain level of robustness against the deadline by tuning the gains (cf., e.g., [16, Chapter 4]). The intention for employing a sliding-mode-like controller is to explicitly cope with the force saturations, which is somewhat different from a common aim of using sliding modes to ensure accurate convergence [1], [13], [17], [18]. In addition, the controller is extended to handle a regenerative pipeline in the hydraulic circuit, which is not explicitly taken into account in the quasistatic actuator model.

The primary novelty of the proposed controller is the differential-algebraic combination of three components; a PD controller, a sliding mode controller, and the quasistatic actuator model [15]. Some robot controllers proposed by Kikuuwe [19], [20] were based on a similar idea, in which only a PD controller and a sliding mode controller were combined. They were only for actuators that do not require elaborate physical models. The proposed controller is built on an combination of the aforementioned three components, which is quite non-trivial because two of the components (except the PD controller) are described by set-valued functions. In addition, as a consequence of incorporating the quasistatic actuator model [15], the proposed controller takes into account all valves, including the check valves and the relief valves. This feature is indeed shared with the authors' previous controller [14] but the inclusion of PD controller, instead of the plant dynamics model, differentiates the proposed controller from this previous controller [14].

Another novelty lies in the extension of the proposed controller, which takes into account the effect of the regenerative pipeline. Its effect is treated in an approximate manner because the quasistatic actuator model [15] does not

take it into account. The effect of the regenerative pipeline has not been addressed in our previous controller [14].

The rest of this paper is organized as follows. Section II provides some preliminaries regarding set-valued functions, related work, the quasistatic actuator model [15], and the authors' previous controller [14]. Section III presents the proposed position controller and its discrete-time algorithm. Section IV provides some analyses on the controller. Sections V and VI show the results of simulations and experiments employing a 13-ton class excavator, respectively. Section VII concludes this paper.

II. PRELIMINARIES

A. Related Work

Several controllers [1], [2], [3], [4] for hydraulic excavators have been proposed based on a locally linearized model of the system. Some of the controllers [1], [2], [3] are based on a time-delay-control approach, in which the uncertain dynamics of the plant are estimated from the measured states, such as actuator torques and joint angles. Kim et al. [4] designed a robust controller based on μ -synthesis with as a second-order plus deadline model of the plant. Gain-tuning methods [5], [6], [7], [8] based on metaheuristic approaches, such as particle swarm optimization and genetic algorithms, have been proposed for linear controllers. To handle the strong nonlinearity of the actuator characteristics, some controllers [9], [10], [11], [12], [13] employ neural networks for the compensation of the nonlinearity. It has been reported that smooth trajectory tracking can be achieved with these controllers, but no controller analytically takes into account the effects of all valves, such as the regenerative pipelines, the force saturation and the square-root law [21] of the pressure-flowrate relation.

It has been reported that the hydraulic systems have large deadline, which is typically 0.1 s to 0.6 s or more [2], [4], [14] in commercial hydraulic excavators. Kim et al. [4] modeled a hydraulic plant as a second-order system with a deadline, which is measured in preliminary experiments, and designed a position controller based on the model. Chang and Lee [2] proposed a position controller with an additional linear controller based on chamber pressures to compensate for the deadline. There are learning-based controllers for hydraulic excavators with deadline [11], [12]. Lee et al. [11] proposed a motion controller based on a data-driven model of the excavators. Egli and Hutter [12] proposed a control approach employing reinforcement learning for excavators with the deadline. These controllers, which explicitly compensate for the deadline, achieve accurate trajectory tracking, but their performance depends on the accuracy of the learning and the identification of the actuator dynamics including the deadline.

Some hydraulic actuators in excavators have auxiliary pipelines known as regenerative pipelines for enhancing task efficiency. These pipelines inject additional complexities to the actuator characteristics. An example of work involving regenerative pipelines is the study by Kim et al. [22]. They proposed a velocity-field controller based on a detailed model

of actuators with regenerative pipelines, but it does not take into account the saturation of the actuator force.

To summarize, among the aforementioned controllers, the deadtime is addressed in [2], [4], [11], [12], and [14] and the nonlinearities of both the control valves and relief valves are considered in [5], [6], [7], [8], and [14]. Thus, only [14], which is the authors' previous paper, considers both the deadtime and the valve effects. It however strongly depends on a priori knowledge on the plant dynamics and the deadtime in the plant. The effect of regenerative pipelines is considered only in [22], in which the relief valve effects are excluded.

B. Mathematical Preliminaries

In this paper, \mathbb{R} denotes the set of all real numbers and \mathcal{B} denotes the closed unit ball in \mathbb{R} , i.e., $\mathcal{B} \triangleq [-1, 1] \subset \mathbb{R}$.

The following functions are used in this paper:

$$\text{sat}_{\mathcal{X}}(x) \triangleq \begin{cases} \min \mathcal{X} & \text{if } x < \min \mathcal{X} \\ x & \text{if } x \in \mathcal{X} \\ \max \mathcal{X} & \text{if } x > \max \mathcal{X} \end{cases} \quad (1)$$

$$\text{sgn}(x) \triangleq \begin{cases} x/|x| & \text{if } x \neq 0 \\ [-1, 1] & \text{if } x = 0 \end{cases} \quad (2)$$

$$\mathcal{R}(x) \triangleq \text{sgn}(x)\sqrt{|x|}. \quad (3)$$

In addition, a function of a set should be understood in the following manner:

$$\Phi(\mathcal{X}) = \bigcup_{x \in \mathcal{X}} \Phi(x). \quad (4)$$

Here, \mathcal{X} is a closed interval in \mathbb{R} . The function \mathcal{R} , which also appears in our previous papers [14], [15], is used to concisely describe the square-root relations [21] between the flowrates and the pressures across valves.

C. Quasistatic Actuator Model

The overall structure of the actuator considered in this paper is illustrated in Fig. 2. As can be seen in the figure, the circuit has a pump, which supplies the oil in the circuit at a flowrate Q . In order to control the hydraulic flow, the circuit is equipped with four main control valves and a bleed valve. The head-side, rod-side, and pump relief valves are for securing the oil outlet, of which the pressure limits are P_{hM} , P_{rM} , and P_M , respectively. This circuit has three check valves to prevent the backflow of the oil. The actuator is divided into two chambers by a piston, of which cross-sectional areas and internal pressures are denoted by A_* and P_* ($* \in \{h, r\}$), respectively (where h means head-side and r means rod-side). The actuator force is lower-bounded by $-F_{rM} \triangleq -A_r P_{rM}$ and upper-bounded by $F_{hM} \triangleq A_h P_{hM}$ due to the effects of the head-side and rod-side relief valves.

The ratio of the opening area to its maximum of each of five control valves (four main control valves and the bleed valve) is denoted by $u_* \in [0, 1]$ ($* \in \{ph, pr, th, tr, b\}$). The flowrates Q_* of the valves satisfy the following flowrate-pressure relations [21], [23]:

$$Q_* = c_* u_* \mathcal{R}(\Delta P_*) \quad (* \in \{ph, tr, th, pr, b\}) \quad (5)$$

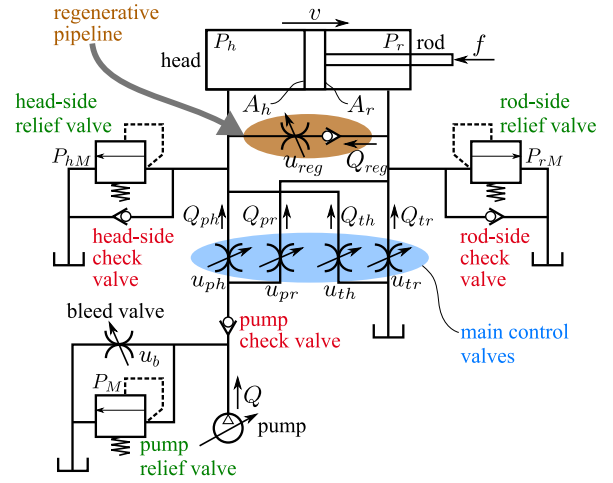


Fig. 2. Hydraulic actuator and its circuit. It is close to the one considered in [14] but the regenerative pipeline is now included.

where $c_* \triangleq C_* a_* \sqrt{2/\rho}$, ΔP_* is the pressure drop across the valve, ρ is the mass density of the oil, a_* is the maximum opening area of the valve, and C_* is its discharge coefficient [24], which is a non-dimensional quantity. It has been known [25], [26] that C_* is typically around 0.6 or 0.7.

The actuators of excavators may have an additional pipeline, referred to as the regenerative pipeline, which is also included in the diagram of Fig. 2. This pipeline is for making the extending motion faster when the actuator is subjected to the tensile external force. Typically, excavators' arm actuators (as opposed to the boom or bucket actuators) possess this architecture to accelerate the arm lowering action. The flowrate through the regenerative pipeline Q_{reg} can be given as follows:

$$Q_{reg} = c_{reg} u_{reg} \max(\mathcal{R}(P_r - P_h), 0) \quad (6)$$

where $c_{reg} \triangleq C_{reg} a_{reg} \sqrt{2/\rho}$, u_{reg} denotes the ratio of the opening area to its maximum, a_{reg} is the maximum opening area of the valve, and C_{reg} is the discharge coefficient [24] of the valve.

Let us now focus on the actuator illustrated in Fig. 2 with the regenerative pipeline being excluded. The previous study [15] presented a quasistatic model of such an actuator. The model is represented by a set-valued function Γ that connects the actuator force $f \in \mathbb{R}$, the rod velocity $v \in \mathbb{R}$, and the control input $u \in \mathcal{B}$ in the following form:

$$f \in \Gamma(v, u). \quad (7)$$

Here, the control input u means the signal that determines the valve opening ratios in the following manner:

$$u_{ph} = u_{tr} = \max(0, u), \quad u_{pr} = u_{th} = -\min(0, u). \quad (8)$$

Note that the control input $u \in \mathcal{B}$ is not to be confused with the valve opening ratios $u_* \in [0, 1]$ ($* \in \{ph, tr, pr, th\}$). The exact analytical form of the set-valued function Γ is presented in [15].

For the use of the model in control and simulation, the function Γ needs to be transformed into some different forms. First, as detailed in [27], we need to have the inverse function Θ of the function Γ with respect to its second argument, which

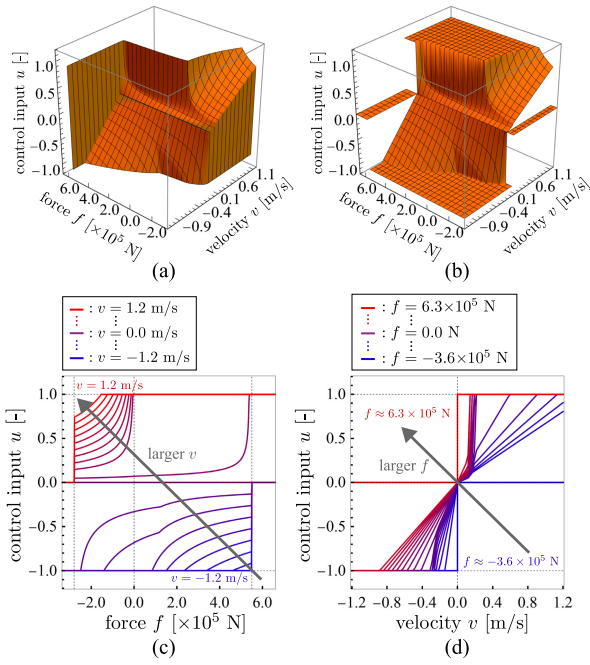


Fig. 3. Graphs of $u \in \Theta(v, f)$ and $u = \Theta_s(v, f)$ representing the actuator model [14], [15], where the control input u determines the opening ratios of the main control valves through (8). (a) Graph of $u \in \Theta(v, f)$ in the v - f - u space. (b) Graph of $u = \Theta_s(v, f)$ in the v - f - u space. (c) Cross-sections of (b) at different velocities $v \in [-1.2 \text{ m/s}, 1.2 \text{ m/s}]$, which are indicated by the line colors ranging from blue to red. (d) Cross-sections of (b) at different forces $f \in [-3.6 \times 10^5 \text{ N}, 6.3 \times 10^5 \text{ N}]$, which are indicated by the line colors ranging from blue to red.

satisfies the following:

$$u \in \Theta(v, f) \iff f \in \Gamma(v, u). \quad (9)$$

Here, note that Θ is also a set-valued function. In addition, we need two single-valued functions Θ_s and Γ_s , which satisfy the following relations:

$$f = \Gamma_s(\eta, v, u) \iff f \in \Gamma(v + \eta f, u) \quad (10)$$

$$\Theta_s(v, f) \in \Theta(v, \text{sat}_{\Gamma(v, \mathcal{B})}(f)) \quad (11)$$

where $\eta > 0$. The analytical forms of the functions Γ_s , Θ_s , and Θ are provided in [14] and [27, Theorem 3]. Fig. 3 shows graphs of Θ_s with the parameter values of the boom actuator used in the simulations in Section V. As can be seen from Fig. 3(a), the function Θ is set-valued at $v = 0$, $f \approx 5.5 \times 10^5$ ($\approx F_{hM}$) or $f \approx -2.8 \times 10^5$ ($\approx -F_{rM}$). The function Θ_s can be seen as a single-valued and domain-extended version of the function Θ . A three-dimensional visualization of the function Θ is shown in Fig. 3(b), and Figs. 3(c) and (d) show the cross-sections in the v - u plane and the f - u plane, respectively. As seen in Figs. 3(c)(d), the control input u is monotone (monotonically increasing) with respect to v and f .

The circuit including the generative pipeline is also modeled in [15] in the quasistatic manner. The actuator model can be written in the following form:

$$f = F_h - F_r \quad (12a)$$

$$F_h \in \Gamma_h(v - Q_{reg}/A_h, u) \quad (12b)$$

$$F_r \in \Gamma_r(v - Q_{reg}/A_r, u) \quad (12c)$$

$$Q_{reg} = c_{reg} u_{reg} \max(\mathcal{R}(F_r/A_r - F_h/A_h), 0). \quad (12d)$$

Here, the functions Γ_h and Γ_r , which are detailed in [15], give the forces generated by the head- and rod-side chambers, respectively, and they satisfy $\Gamma(v, u) = \Gamma_h(v, u) - \Gamma_r(v, u)$. The quantities Q_{reg} , F_r , and F_h are determined by the algebraic constraints (12b), (12c), and (12d), and the algorithm of iterative computation to provide the solutions has been provided in [15]. This paper does not attempt to directly use it because of its high computational cost for the iterative computation. Instead, this paper uses an approximate, simplified form of the model inspired by the representation (12), which will be presented in Section III-D.

D. Previous Controller Using Quasistatic Actuator Model

In the previous paper [14], the authors proposed a set-point position controller for hydraulic excavator based on the quasistatic actuator model [15] overviewed in Section II-C. The controller was intended to be applied to the class of plants that are described as follows:

$$M\dot{v} = f + g \quad (13a)$$

$$\dot{p} = v \quad (13b)$$

$$f \in \Gamma(v, u) \quad (13c)$$

where $M > 0$ is the mass of the controlled object, $p \in \mathbb{R}$ and $v \in \mathbb{R}$ are the position and the velocity of the object, respectively, $f \in \mathbb{R}$ is the actuator force and $g \in \mathbb{R}$ is the external force acting to the object. The function Γ is the quasistatic actuator model discussed in Section II-C, and its second argument $u \in \mathcal{B}$ is the control input that should be given from a controller.

The previous controller [14] was constructed from the following continuous-time representation:

$$M\ddot{p} = \hat{f} + \hat{g} \quad (14a)$$

$$\hat{f} \in \Gamma(\dot{p}, \text{sgn}(p_d - p + H(\dot{p}_d - \dot{p}))) \quad (14b)$$

$$u \in \Theta(v, f) \quad (14c)$$

where p_d is the target position, \hat{g} is an estimated external force, \hat{f} is an intended actuator force, and H is a parameter to determine the time constant of the convergence. Here, note that the equation (14a) is the nominal model of the controlled object (13a). The control input u is determined by an algorithm derived from the implicit-Euler discretization of (14) based on a mathematical framework detailed in [27].

To deal with the deadtime in the hydraulic actuator, the controller (14) in [14] was combined with a state predictor based on a nominal plant model, which is of the form of (13). It requires a predetermined look-ahead time \hat{T}_d , which should be set as close as possible to the deadtime, and the position and velocity of the time \hat{T}_d future are predicted by the simple time integration of the nominal model of the form (13). The drawback of this approach is its strong dependency on the accuracy of the model, especially on the nominal inertia M .

III. PROPOSED CONTROLLER

A. Continuous-Time Representation

This paper also intends to develop a controller for the class of plants described as (13). We propose a position

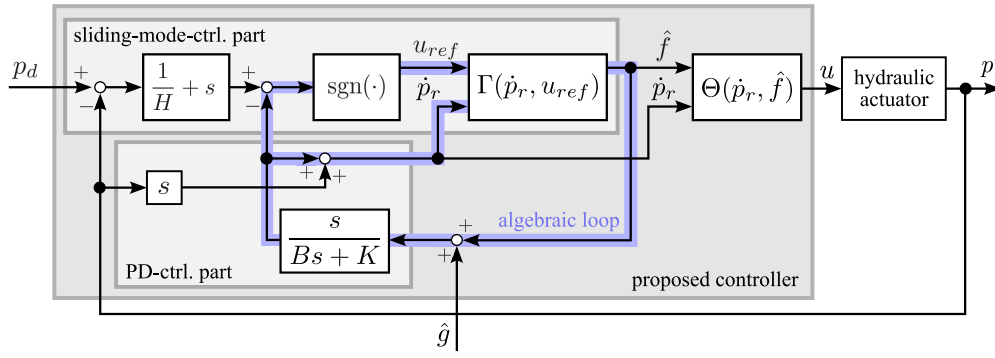


Fig. 4. Block diagram of the proposed controller. The set-valued functions Γ and Θ are determined according to the structure of the hydraulic circuit.

controller whose continuous-time representation can be written as follows:

$$\hat{f} = K(p_r - p) + B(\dot{p}_r - \dot{p}) - \hat{g} \quad (15a)$$

$$\hat{f} \in \Gamma(\dot{p}_r, \text{sgn}(p_d - p + H(\dot{p}_d - \dot{p}_r))) \quad (15b)$$

$$u \in \Theta(\dot{p}_r, \hat{f}). \quad (15c)$$

The inputs to the controller are the target position p_d , the measured position p , and the estimated external force \hat{g} . The output from the controller is the control input $u \in \mathcal{B}$. The controller possesses a state variable p_r , which can be seen as a reference position. The variable \hat{f} can be interpreted as the intended actuator force, which is not a state variable but a function of the state variable and the inputs.

The main parts (15a) and (15b) of the controller constitute a set of differential-algebraic constraints that determines \dot{p}_r and \hat{f} . This set of differential-algebraic constraints appears as an algebraic loop in the block diagram of Fig. 4. The obtained values are used in (15c) to determine the control input u . The controller algorithm to solve these constraints is derived through the implicit-Euler discretization as detailed in the next Section III-C.

In the proposed controller (15), the components (15a) and (15b) can be seen as a PD controller and a sliding-mode-like controller, respectively. The PD controller (15a), with the proportional gain of K and the derivative gain B , is intended to make the position p track the reference position p_r . The sliding-mode-like controller (15b) is to make the position p exponentially converge to the target position p_d with the time constant H .

B. Properties of the Controller

Some properties of the controller (15) are now discussed. By setting $e \triangleq p_r - p$, we can rewrite (15) as follows:

$$\dot{e} = (\hat{f} + \hat{g} - Ke)/B \quad (16a)$$

$$\hat{f} \in \Gamma(\dot{p} + \dot{e}, \text{sgn}(-\sigma/H - \dot{e})) \quad (16b)$$

$$u \in \Theta(\dot{p} + \dot{e}, \hat{f}) \quad (16c)$$

where $\sigma \triangleq p - p_d + H(\dot{p} - \dot{p}_d)$.

In the extreme case of $B \rightarrow \infty$, (16a) reduces to $\dot{e} = 0$, and thus the whole controller (16) reduces to the following:

$$u \in \Theta(\dot{p}, \Gamma(\dot{p}, \text{sgn}(-\sigma/H))). \quad (17)$$

The controller (17) can be seen as a sliding mode controller with the sliding surface $\sigma = 0$, which is a variant of the one discussed in [27, Section IV.A].

Our previous controller [14], overviewed in Section II-D, was also derived from the sliding-mode controller (17), but it is algebraically combined with the plant dynamics model (14a). In contrast, the proposed controller is derived by combining (17) with the PD controller (15a). This difference is beneficial in that the proposed controller is less dependent on the plant dynamics model, which is not usually accurately available, and also in that the influence of the deadtime can be reduced to a certain level by appropriately tuning the PD gains, as has been discussed in, e.g., [16, Section 4.2]. It should be noted that the proposed controller does not incorporate explicit compensation for the deadtime, while the previous controller [14] required a deadtime compensation using a state predictor depending on a precalibrated look-ahead time \hat{T}_d .

Similar approaches combining a sliding-mode controller and a PD controller have been presented by Kikuuwe et al. [19], [20]. Their controllers are originally intended for mechatronics systems with electromagnetic actuators, to which the forces to be generated can be directly commanded. The very initial idea of the proposed controller was to combine the concept of Kikuuwe et al.'s [19] controller with the quasistatic model [15] of hydraulic actuators, but some modifications were needed to adapt it to the particular structure of the quasistatic actuator model [15]. Specifically, the sliding surface is approximated to $p_d - p_r + H(\dot{p}_d - \dot{p}_r) = 0$ in [19], while to $p_d - p + H(\dot{p}_d - \dot{p}_r) = 0$ in this paper. Because the proposed controller uses \dot{p}_r as the first argument of Θ in (15c), $\dot{p}_r = 0$ results in $u = 0$. This means that the use of p_r in the sliding surface results in $u = 0$ when p_d is reached by p_r , not by p . This is the reason why the proposed controller uses the sliding surface comprising p , not p_r .

C. Discrete-Time Implementation

Now we derive a discrete-time algorithm of the controller (15) through the implicit Euler discretization. For the convenience of derivation, let us rewrite (15) as follows:

$$\hat{f} = Ke + B\dot{e} - \hat{g} \quad (18a)$$

$$\hat{f} \in \Gamma(v_r, \text{sgn}(p_d - p + H(v_d - v_r))) \quad (18b)$$

$$u \in \Theta(v_r, \hat{f}) \quad (18c)$$

$$\dot{e} = v_r - v, \quad \dot{p}_r = v_r, \quad \dot{p}_d = v_d. \quad (18d)$$

$$u \in \Theta(\dot{p}_r - v_{reg}(\dot{p}_r, u_{reg}, \hat{g}), \hat{f}). \quad (25c)$$

Fig. 5 shows the overall structure of the controller (25). We here assume that u_{reg} , the valve opening ratio of the regenerative pipeline, is determined by the internal, built-in controller of the actuator, and thus cannot be manipulated by our controller. We however assume that, as shown in Fig. 5, u_{reg} is readable from our controller. We also assume that the estimated tensile external force \hat{g} is available by some estimation methods, such as those based on the gravity calculated from the nominal masses of the links.

In a similar manner as we derived (22) from (15), one can obtain a discrete-time implementation of (25) as follows:

$$v_k := (p_k - p_{k-1})/T \quad (26a)$$

$$v_{d,k} := (p_{d,k} - p_{d,k-1})/T \quad (26b)$$

$$v_{k,reg} := v_{reg}(v_{r,k-1}, u_{reg,k}, \hat{g}_k) \quad (26c)$$

$$v_{s,k} := (p_{d,k} - p_k + H v_{d,k})/H \quad (26d)$$

$$v_{f,k} := v_k - (K e_{k-1} - \hat{g}_k)/A \quad (26e)$$

$$\hat{f}_k := \text{sat}_{\Gamma_s(1/A, v_{f,k} - v_{k,reg}, \mathcal{B})}(A(v_{s,k} - v_{f,k})) \quad (26f)$$

$$v_{r,k} := v_{f,k} + \hat{f}_k/A \quad (26g)$$

$$e_k := e_{k-1} + (v_{r,k} - v_k)T \quad (26h)$$

$$u_k := \Theta_s(v_{r,k} - v_{k,reg}, \hat{f}_k). \quad (26i)$$

Note that the only difference of the algorithm (26) from the algorithm (22) is the subtraction of $v_{k,reg}$ from $v_{f,k}$ in (26f) and (26i), and when $v_{k,reg}$ is set zero, (26) reduces to (22).

IV. SOME ANALYSES

A. Stability Analysis

This section shows a stability analysis of the proposed controller (15) applied to the plant (13). Recall that the controller (15) can be equivalently rewritten as (16). The closed-loop system composed of the plant (13) and the controller (16) can be written as follows:

$$\sigma = p - p_d + H(v - \dot{p}_d) \quad (27a)$$

$$\dot{e} = (\hat{f} + \hat{g} - K e)/B \quad (27b)$$

$$\dot{v} = (f + g)/M \quad (27c)$$

$$v_r = v + \dot{e} \quad (27d)$$

$$f \in \Gamma(v, \Theta(v_r, \hat{f})) \quad (27e)$$

$$\hat{f} \in \Gamma(v_r, \text{sgn}(-\sigma/H - \dot{e})). \quad (27f)$$

Here, we introduce the following functions $\tilde{\Gamma}$ and $\bar{\beta}$:

$$\tilde{\Gamma}(b, v_r, \hat{f}) \triangleq \Gamma(v_r - b, \Theta(v_r, \hat{f})) - \hat{f} \quad (28)$$

$$\bar{\beta}(b, v_r, \hat{f}) \triangleq \begin{cases} \frac{\tilde{\Gamma}(b, v_r, \hat{f})}{b} & \text{if } b \neq 0 \\ \min\left(\lim_{b \rightarrow 0^+} \frac{\tilde{\Gamma}(b, v_r, \hat{f})}{b}, \lim_{b \rightarrow 0^-} \frac{\tilde{\Gamma}(b, v_r, \hat{f})}{b}\right) & \text{otherwise.} \end{cases} \quad (29)$$

By employing the function (29) and the relation (21), we can rewrite the system (27) as follows:

$$\dot{\sigma} = v - \dot{p}_d + H(\dot{v} - \ddot{p}_d) \quad (30a)$$

$$\dot{e} = (\hat{f} + \hat{g} - K e)/B \quad (30b)$$

$$\dot{v} = (\hat{f} + \beta \dot{e} + g)/M \quad (30c)$$

$$\hat{f} = \text{sat}_{\Gamma_s(1/B, v - (K e - \hat{g})/B, \mathcal{B})}(-B\sigma/H + K e - \hat{g}) \quad (30d)$$

where

$$\beta = \bar{\beta}(\dot{e}, v + \dot{e}, \hat{f}). \quad (31)$$

At present, although it is not very conclusive, we have the following result in regard to properties of the closed-loop system (30):

Theorem 1: With the system (30), the state $[\sigma, v - \dot{p}_d, e]^T$ is uniformly ultimately bounded [28, Definition 4.6] if there exist $\delta > 0$ and $\alpha > 0$ with which

$$M < B(B + HK)/K \quad (32a)$$

$$\delta \mathcal{B} \subset \Gamma_s(1/B, \dot{p}_d + \hat{g}/B, \mathcal{B}) + \hat{g} \quad (32b)$$

$$|g - \hat{g} - M \ddot{p}_d| < \alpha \quad (32c)$$

are satisfied, α is sufficiently small, and $|\dot{\beta}|$ is sufficiently small. In addition, if $g \equiv \hat{g}$ and $\ddot{p}_d \equiv 0$ are satisfied as well, the origin $[\sigma, v - \dot{p}_d, e]^T = 0$ is asymptotically stable.

The proof of Theorem 1 is provided in Appendix. The requirement that $|\dot{\beta}|$ should be sufficiently small may or may not be restrictive and at least it hampers the completeness of the result. The incompleteness stems from the fact that the dynamics of β is not fully analyzed in the proof. It leaves the possibility that some particular patterns of temporal changes in β might make the state diverge. It however does not seem likely in practice considering that the term with β acts as a damping term that dissipates the energy. A more thorough proof considering the dynamics of β remains as an open problem to be addressed.

It should be noted that Theorem 1 is to be understood as a baseline assurance, which is prerequisite for practical application of the controller, and is not very useful for parameter tuning purposes. The condition (32) is a conservative sufficient condition, of which the violation does not necessarily mean the instability. Less conservative conditions, which could be useful as a predictive tool for parameter tuning, may need to be sought in the future study.

B. Parameter Tuning

This section provides some analyses that can be used for tuning the parameters $\{K, B, H\}$ of the controller (15). We employ another equivalent form (16) of the controller (15) for discussing the parameter tuning. Let us consider the case where the control input u is not saturated, i.e., the case where $-\sigma/H - \dot{e} = 0$ is satisfied. In this case, the intended actuator force \hat{f} and the state variable \dot{p}_r of the controller (16) are determined to satisfy both $-\sigma/H - \dot{e} = 0$ and (16a). Therefore, in this case, we can rewrite the controller (16) as follows:

$$\hat{f} = K_a(p_d - p) + B(v_d - v) + L_a \int (p_d - p)dt - \hat{g} \quad (33a)$$

$$v_r = v_d + (p_d - p)/H \quad (33b)$$

$$u \in \Theta(v_r, \hat{f}) \quad (33c)$$

$$\dot{p}_r = v_r, \quad \dot{p} = v, \quad \dot{p}_d = v_d \quad (33d)$$

where $K_a \triangleq K + B/H$ and $L_a \triangleq K/H$. The intended actuator force \hat{f} is determined by the PID controller (33a). The state variable v_r is determined by the positional error $p_d - p$ and the target velocity \dot{p}_d .

We consider the closed-loop system composed of the controller (33) and the plant (13) with deadtime T_d because the hydraulic systems of commercial excavators are known to involve some deadtime [2], [4], [14]. The closed-loop system can be expressed as follows:

$$\hat{f} = K_a(p_d - p) + B(v_d - v) + L_a \int (p_d - p)dt - \hat{g} \quad (34a)$$

$$v_r = v_d + (p_d - p)/H \quad (34b)$$

$$f \in \Gamma(v(t + T_d), \Theta(v_r, \hat{f})) \quad (34c)$$

$$M\dot{v}(t + T_d) = f + g. \quad (34d)$$

Here, variables without arguments are functions of time t but the argument t is omitted for brevity.

Let us assume that, with $\{v_r, \hat{f}\}$ in (34c), $\Theta(v_r, \hat{f})$ is single-valued, and that $\Theta(v_r, \hat{f}) \in [-1, 1]$ and $\hat{f} \in [-F_{rM}, F_{hM}]$ hold true. Then, from the first-order Taylor expansion of $\Gamma(v, \Theta(v_r, \hat{f}))$ with respect to v around $v = v_r$, the following approximation holds:

$$\Gamma(v, \Theta(v_r, \hat{f})) \approx \hat{f} + \kappa(v_r, \hat{f})(v_r - v) + \mathcal{O}((v_r - v)^2) \quad (35)$$

where

$$\kappa(v_r, \hat{f}) \triangleq - \left. \frac{\partial \Gamma(v, u)}{\partial v} \right|_{v=v_r, u=\Theta(v_r, \hat{f})}. \quad (36)$$

Due to the properties of the function Γ discussed in [15], $\kappa(v_r, \hat{f}) \geq 0$ is always satisfied. Eliminating f and \hat{f} from (34) by using the approximation (35) and assuming $\hat{g} = g$, we can rewrite the system (34) as following:

$$\begin{aligned} M\dot{v}(t + T_d) &= K_a(p_d - p) + B(v_d - v) \\ &+ L_a \int (p_d - p)dt + \kappa(v_r, \hat{f})(v_r - v(t + T_d)). \end{aligned} \quad (37)$$

Eq. (37) means that the controlled object is driven by a PID controller with an additional viscosity-like term. Assuming κ is constant, we can obtain the transfer function $G(s)$ of the system (37) as follows:

$$\begin{aligned} G(s) &= \frac{\mathcal{L}[p]}{\mathcal{L}[p_d]} \\ &= \frac{(Hs + 1)(s(\kappa + B) + K)}{HMe^{sT_d}s^3 + (\kappa e^{sT_d} + B)Hs^2 + (\kappa + B + HK)s + K} \end{aligned} \quad (38)$$

where \mathcal{L} represents the Laplace transform.

The pole locations of the transfer function $G(s)$ in (38) can be used for tuning the parameters $\{K, B, H\}$ because they represent the response characteristics of the system. In particular, for achieving smooth convergence without overshoots, the poles should be located on the real axis in the left-half plane. In order to obtain the poles, one needs to

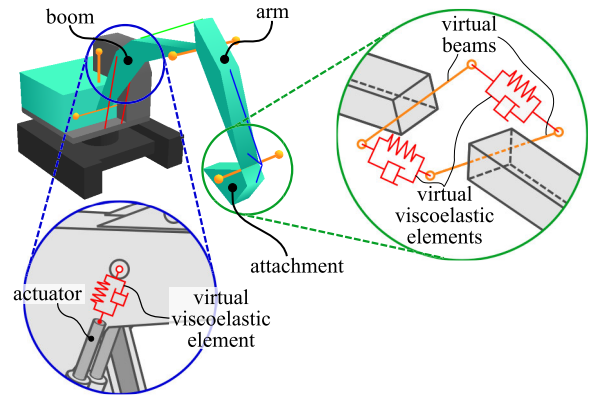


Fig. 6. Connections among links and actuators in the simulator, through virtual viscoelastic elements. The virtual viscoelastic elements emulate the compressibility of the oil in the actuators and the compliance of the links.

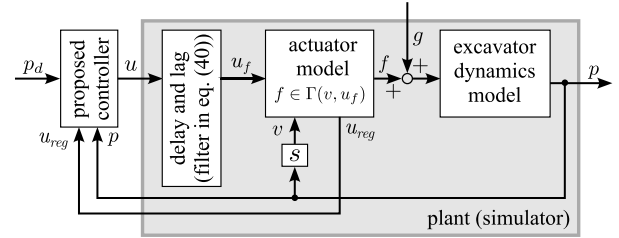


Fig. 7. Simulation setup. The actuator force f is calculated by the function Γ representing a quasistatic actuator model [15]. The opening ratio u_{reg} of the regenerative pipeline is determined by the built-in controller of the actuator and is used in the proposed controller, i.e., the algorithm (26).

set an appropriate value to κ , which is the sign-reversed slope of the function Γ in the v direction. As has been detailed in previous papers [14], [27], the set-valued function Γ satisfies $\Gamma(0, 0) = [-F_{hM}, F_{rM}]$ and it is monotone with respect to $-v$ (i.e., monotonically decreasing with respect to v). Therefore, to investigate the system behavior around the equilibrium $p_d = p \wedge v = 0$, a possible choice of κ can be given as follows:

$$\kappa \approx \frac{F_{rM} + F_{hM}}{\Delta v} \quad (39a)$$

where

$$\Delta v \triangleq \frac{\min(F_{rM}, F_{hM})T}{M}. \quad (39b)$$

Here, Δv can be seen as the maximum velocity that can be reached within the sampling interval T from $v = 0$, and thus $-\kappa$ can be seen as an effective slope value of $\Gamma(v, u)$ around $v = 0 \wedge u = 0$ in the discrete-time domain. Section V-B will present some numerical examples and simulation results supporting this approach.

V. SIMULATIONS

A. Setup

A realtime simulator of a 13-ton class hydraulic excavator was employed to validate the proposed controller. The simulator was constructed with Microsoft Visual C++ and the controller was constructed with MATLAB/Simulink. They were connected to each other through UDP/IP sockets at the

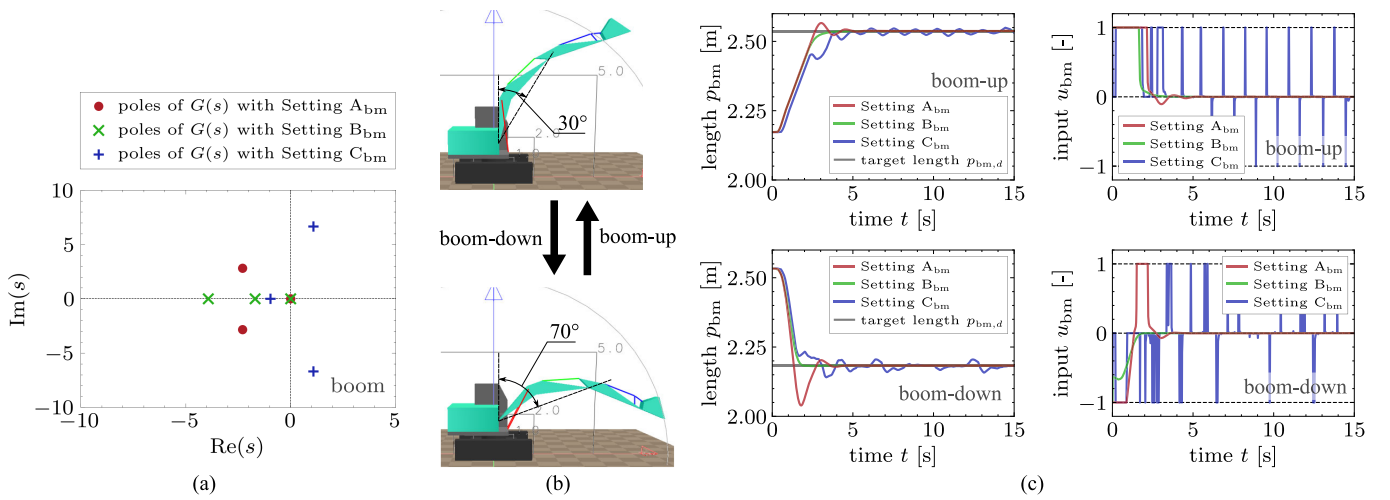


Fig. 8. Simulation of step responses of the boom actuator with three different parameter settings, which are Settings A_{bm}, B_{bm}, and C_{bm} shown in Section V-B. (a) Poles of the transfer function $G(s)$ in (38). (b) Configuration of the excavator. (c) Step responses of the boom.

TABLE I
PARAMETERS OF THE HYDRAULIC
ACTUATORS IN THE SIMULATOR

symbols	physical meanings	boom	arm
P_{hM}	pressure limit of the head-side relief valves	35 MPa	35 MPa
P_{rM}	pressure limit of the rod-side relief valves	35 MPa	35 MPa
P_M	pressure limit of the pump relief valve	35 MPa	35 MPa
Q	oil flowrate from the pump	$3.7 \times 10^{-3} \text{ m}^3/\text{s}$	$2.0 \times 10^{-3} \text{ m}^3/\text{s}$
a_{ph}	MA ¹ of MCV ² connected to the pump and the head-side chamber	$1.9 \times 10^{-4} \text{ m}^2$	$2.6 \times 10^{-5} \text{ m}^2$
a_{pr}	MA ¹ of MCV ² connected to the pump and the rod-side chamber	$1.7 \times 10^{-5} \text{ m}^2$	$1.5 \times 10^{-4} \text{ m}^2$
a_{tr}	MA ¹ of MCV ² connected to the tank and the head-side chamber	$6.5 \times 10^{-5} \text{ m}^2$	$6.2 \times 10^{-5} \text{ m}^2$
a_{th}	MA ¹ of MCV ² connected to the tank and the rod-side chamber	$7.2 \times 10^{-5} \text{ m}^2$	$1.5 \times 10^{-4} \text{ m}^2$
a_b	MA ¹ of the bleed valve	$1.8 \times 10^{-4} \text{ m}^2$	$1.5 \times 10^{-4} \text{ m}^2$
u_b	ratio of the bleed valve opening area	0.1	0.1
C_*	discharge coefficients (* $\in \{ph, pr, tr, th, b\}$)	0.7	0.7
ρ	mass density of the oil	850 kg/m ³	850 kg/m ³

¹ MA stands for the maximum opening area.

² MCV stands for a main control valve.

cycle of 10 ms, i.e., the controller's sampling interval was $T = 10$ ms. The simulator's timestep size was 0.1 ms.

In the simulator, the links of the excavator, i.e., the boom, the arm, and the attachment as shown in Fig. 6, were treated as rigid bodies connected through virtual viscoelastic elements and virtual beams as illustrated in the green circle in Fig. 6. The stiffness and the viscosity of the virtual viscoelastic elements were 5.0×10^7 N/m and 3.0×10^5 N·s/m, respectively, and the length of the virtual beams was 2.0 m. The frictions in the joints were implemented by the technique presented in [29].

Each of actuators in the simulator was driven by a hydraulic circuit of the structure illustrated in Fig. 2. The circuit of the arm actuator included the regenerative pipeline, while those of the other three, the swing, the boom, and the attachment actuators, did not. The forces of the actuators were calculated based on the quasistatic actuator model [15]. Some parameters of the actuators are shown in Table I. The actuators were connected to the links through a virtual viscoelastic element with the stiffness 5.0×10^7 N/m and the viscosity 3.0×10^5 N·s/m as illustrated in the blue circle in Fig. 6, employing the technique presented in [30].

In order to emulate the deadtime and the lag in the responses of the main control valves of the actuators, the following filter was installed between the controller and the actuator as shown in Fig. 7:

$$u_f = \mathcal{L}^{-1} \left[\frac{\omega_0^2 e^{-T_d s} \mathcal{L}[u]}{s^2 + 2\zeta \omega_0 s + \omega_0^2} \right] \quad (40)$$

where T_d denotes the deadtime in the hydraulic system. The deadtime was set as $T_d = 0.3$ s. The filter (40) represents the combination of a second-order lag and the deadtime T_d in the response of the main control valves, where we set $\omega_0 = 94.2 (\approx 30\pi)$ rad/s and $\zeta = 1$.

As has been stated in Section III-D, the valve opening ratio u_{reg} of the regenerative pipeline of the arm actuator is assumed to be determined by a built-in controller and is assumed to be available to our position controller. In the simulations, to determine u_{reg} , we used a proprietary algorithm of the built-in controller provided by Kobelco Construction Machinery Co. Ltd., of which the details are not reported here.

B. Step Responses

We conducted some simulations to investigate the effect of the poles of the transfer function $G(s)$ in (38) in Section IV-B. In the simulations, step inputs of the target position p_d were provided to each of the boom and arm controllers with three different parameter settings. The gravitational forces calculated from the mass parameters of each link were employed as the

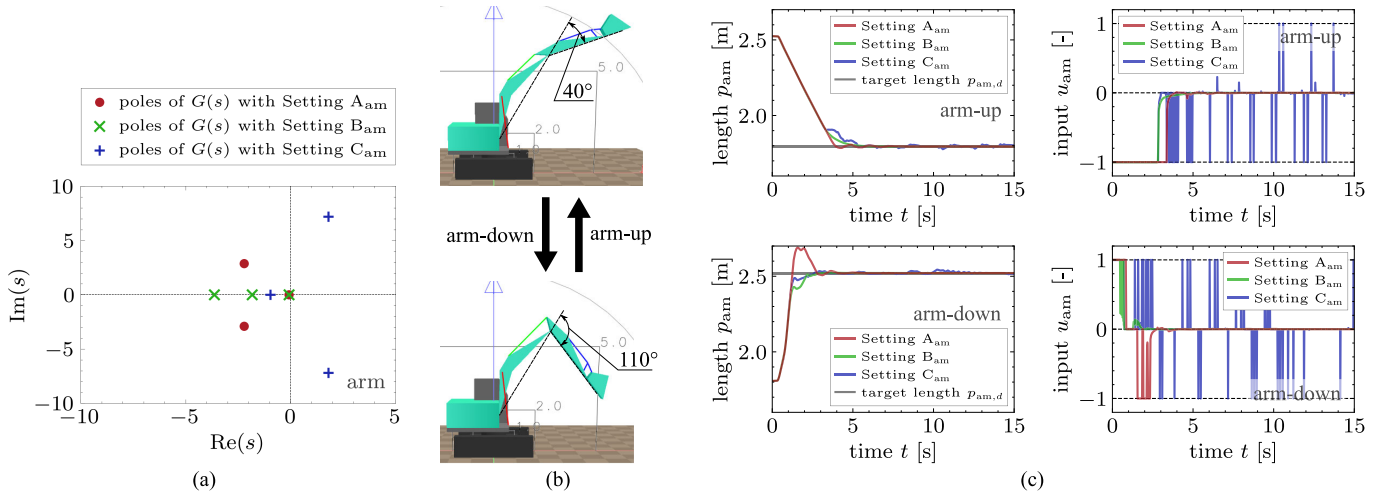


Fig. 9. Simulation of step responses of the arm actuator with three different parameter settings, which are Settings A_{am}, B_{am}, and C_{am} shown in Section V-B. (a) Poles of the transfer function $G(s)$ in (38). (b) Configuration of the excavator. (c) Step responses of the arm.

external forces \hat{g} of the boom and arm controllers. For the boom controller, the following settings were used:

- Setting A_{bm}: $K = 2.5 \times 10^5$ N/m, $B = 2.5 \times 10^2$ N·s/m, $H = 0.5$ s.
- Setting B_{bm}: $K = 2.5 \times 10^5$ N/m, $B = 2.5 \times 10^2$ N·s/m, $H = 1.0$ s.
- Setting C_{bm}: $K = 5.0 \times 10^8$ N/m, $B = 2.5 \times 10^2$ N·s/m, $H = 1.0$ s.

For the arm controller, the following settings were used:

- Setting A_{am}: $K = 1.5 \times 10^6$ N/m, $B = 2.0 \times 10^4$ N·s/m, $H = 0.5$ s.
- Setting B_{am}: $K = 1.5 \times 10^6$ N/m, $B = 2.0 \times 10^4$ N·s/m, $H = 1.0$ s.
- Setting C_{am}: $K = 1.5 \times 10^8$ N/m, $B = 2.0 \times 10^4$ N·s/m, $H = 1.0$ s.

The inertia M in the transfer function $G(s)$ in (38) were set as follows:

$$\hat{M}_* = \frac{I_*}{J_*(\theta_*)^2} \quad (41)$$

where $J_*(\theta_*) \triangleq \partial \Psi_*(\theta_*) / \partial \theta_*$ ($* \in \{\text{bm}, \text{am}\}$) and I_* are the total moments of inertia of the links around the actuator. The function Ψ_* is the kinematics from the joint angle θ_* to the actuator length p_* . The quantity \hat{M}_* can be seen as an equivalent mass of the link seen from the actuator. We employed the equivalent masses \hat{M}_* at the joint angles $\theta_{\text{bm}} = 70^\circ$ and $\theta_{\text{am}} = 40^\circ$, which were $\hat{M}_{\text{bm}} = 2.5 \times 10^5$ kg and $\hat{M}_{\text{am}} = 6.25 \times 10^4$ kg. We used $T_d = 0.3$ s for the transfer function $G(s)$ in (38) and used the first-order Padé approximation to approximate $G(s)$ by a rational function.

Figs. 8(a)(b)(c) show the relations among pole locations and step responses of the boom actuator. Fig. 8(a) shows the pole locations of the boom-actuator system with three parameter settings. Fig. 8(b) illustrates two motions of the step-response simulations, which are the boom-up and boom-down motions. Fig. 8(c) shows their results. From Fig. 8(c), one can see that Setting B_{bm} is the most suitable among the three settings because the actuator length p_b converged to the target length $p_{d,b}$ without overshoots or oscillations. The smooth and overdamped response of Setting B_{bm} in Fig. 8(c) is

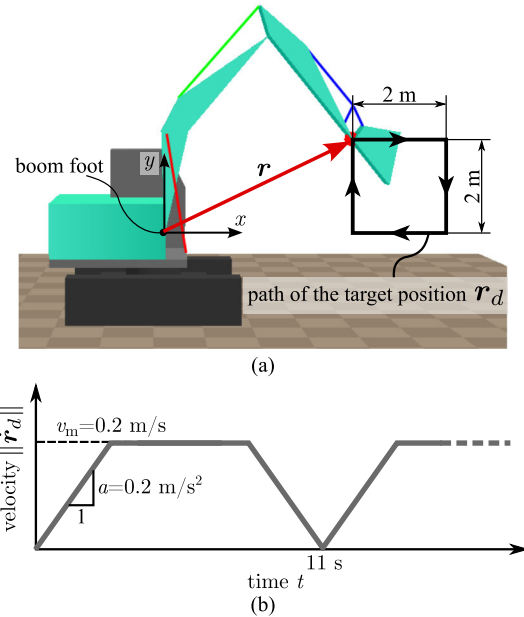


Fig. 10. Target trajectory $r_d(t)$; (a) the trajectory of $r_d(t)$ and the coordinate system, (b) the target velocity $\|r_d\|$, which is triangular.

consistent with the green poles in Fig. 8(a) located on the real axis in the left-half plane. In contrast, Setting A_{bm} resulted in overshoots in Fig. 8(c), and it is consistent with the red poles in Fig. 8(a) in the left-half plane away from the real axis. With Setting C_{bm}, the response became oscillatory though not divergent in Fig. 8(c), and the correspondent poles in Fig. 8(a) are unstable, in the right-half plane. The non-divergent results may be explained by the saturations of the control input $u \in [-1, 1]$ and the actuator force $f \in [-F_{rM}, F_{hM}]$.

Fig. 9(a)(b)(c) show the relations among pole locations and step responses of the arm actuator. Fig. 9(a) shows the pole locations of the arm-actuator system with three parameter settings. Fig. 9(b) illustrates two motions of the step-response simulations, which are the arm-up and arm-down motions. Fig. 9(c) shows their results. It shows that Setting B_{am} resulted

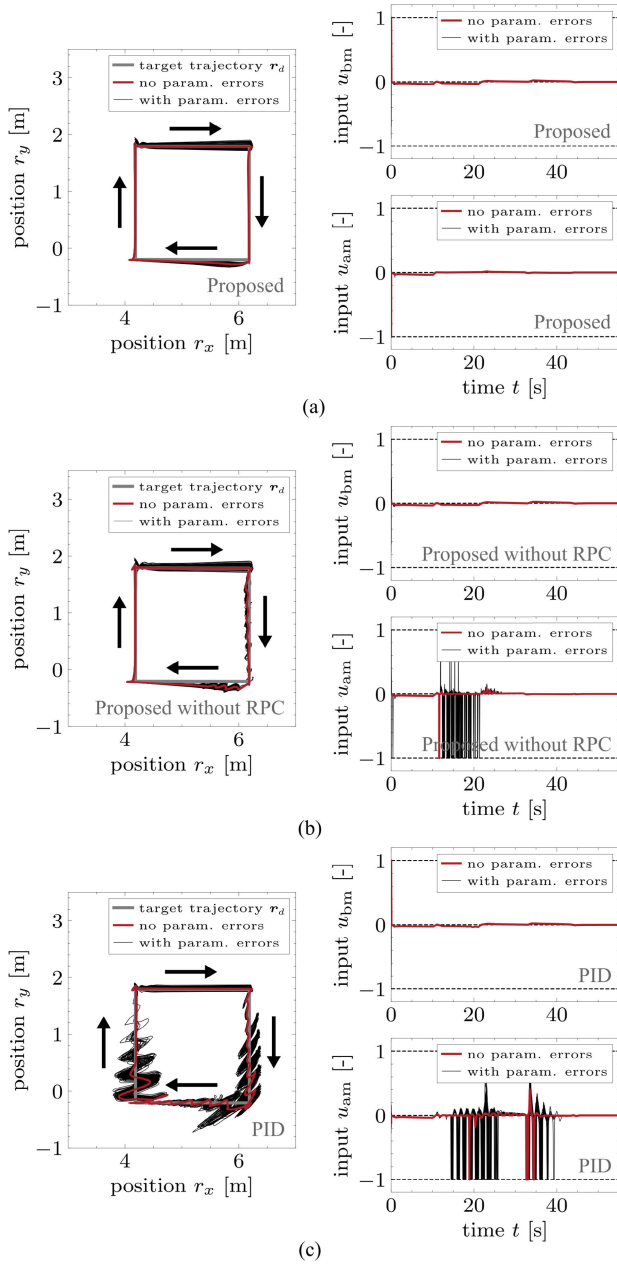


Fig. 11. Simulation results with modeling errors that were randomly selected in $\{-10\%, 0, +10\%$ for parameters of the actuators. The red lines show an almost ideal case with no modeling errors. The number of trials was 100 for each configuration. The deadline T_d was set as 300 ms. (a) The proposed controller. (b) The proposed controller without the regenerative-pipeline compensation (RPC). (c) PID controller (42).

in the most favorable behaviors in both arm-up and arm-down motions. These results are consistent with the locations of the green poles in Fig. 9(a), as has been the case with the results with boom motions. One can see that Setting B_{am} produced small fluctuation in p_{am} in $t \in [1 \text{ s}, 2 \text{ s}]$ of the arm-down motion, which can be attributed to the inaccuracy of the compensation of the regenerative pipeline's effect. The responses with Setting A_{am} in Fig. 9(c) results in overshoots, which are consistent with the red poles away from the real axis shown in Fig. 9(a). As has also been the case with the boom results, from Fig. 9(c), Setting C_{am} resulted in oscillatory responses, although its blue poles in Fig. 9(a) are unstable. It can be attributed to the saturations of u and f .



Fig. 12. Kobelco 13-ton class excavator with a shear attachment.

C. Effects of Errors in the Actuator Models

Some simulations were conducted to test the influence of parametric errors in the actuator models. The modeling errors were generated by randomly varying all actuator parameters including those in Table I by -10% , 0 , or $+10\%$, and the number of trials for each controller was 100. We tested three controllers, which were the proposed controller with the regenerative-pipeline compensation, that without the regenerative-pipeline compensation, and the following PID controller:

$$\hat{f} = K_a(p_d - p) + B(\dot{p}_d - \dot{p}) + L_a \int (p_d - p) dt - \hat{g} \quad (42a)$$

$$v_r = \dot{p}_d + (p_d - p)/H \quad (42b)$$

$$u = \Theta_s(v_r, \hat{f}) \quad (42c)$$

where $K_a \triangleq K + B/H$ and $L_a \triangleq K/H$. Note that, as has been shown in Section IV-B, the PID controller (42) is equivalent to the proposed controller (15) when u and \hat{f} are unsaturated.

The simulations were performed as illustrated in Fig. 10(a), in which the target position r_d was moved along a square trajectory. The velocity $\|\dot{r}_d\|$ was set triangular as shown in Fig. 10(b). The controllers were implemented to each of the boom and the arm actuators, and the target length $\{p_{bm,d}, p_{am,d}\}$ of the actuators were computed through the inverse kinematics from the target arm-tip position r_d . The controller parameters were chosen as the same as Settings B_{bm} and B_{am} , which provided favorable pole placements and step-response results in Section V-B.

Figs. 11(a) and (b) show results with the proposed controller with and without the regenerative-pipeline compensation, respectively. In all cases, the position r converged to the target position r_d . From the comparison between the almost ideal case (the red line) in Fig. 11(a) and that in Fig. 11(b), one can see that the regenerative-pipeline compensation reduces the positional errors. The chattering-like behavior of the control input u_{am} in Fig. 11(b) may be because the total modeling errors may have been too large for the controller without compensation for the regenerative pipeline.

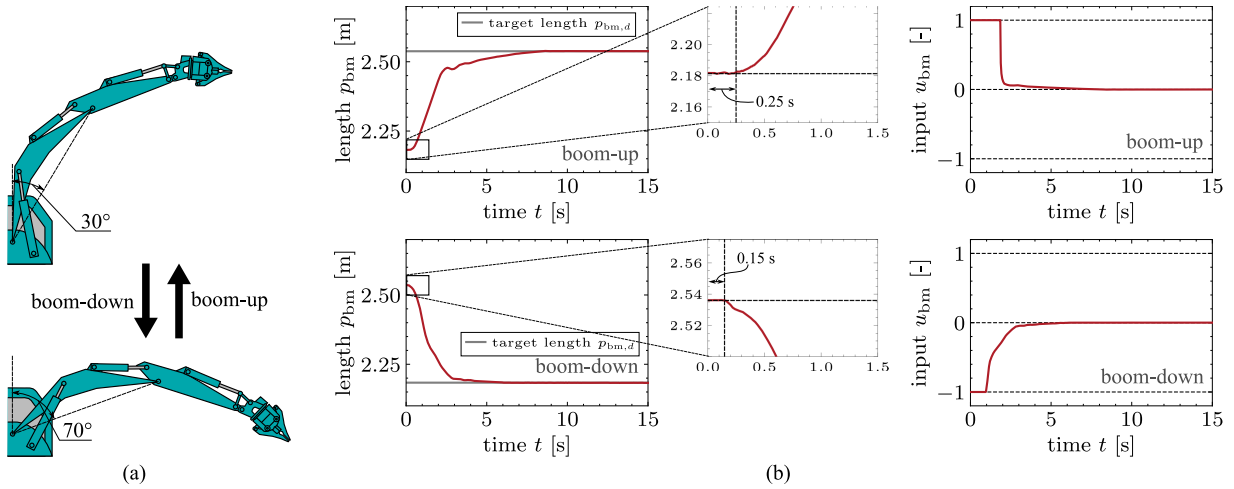


Fig. 13. Experiments of step responses of the boom actuators; (a) Configuration of the excavator and (b) step responses of the boom.

Fig. 11(c) shows simulation results with the PID controller (42). The comparison between Fig. 11(b) and Fig. 11(c) suggests that the proposed controller, even without the regenerative-pipeline compensation, resulted in higher accuracy and smaller oscillations than the PID controller (42). Recalling that (42) is equivalent to the proposed controller (15) as long as \hat{f} and u are unsaturated and considering that the regenerative pipeline acts as a modeling error, one can see that the sliding-mode structure of the proposed controller, which is intended to handle the saturation, contributes to higher robustness against modeling errors.

VI. EXPERIMENTS

A. Setup

We tested the proposed controller with a 13-ton class excavator, Kobelco SK135SRD-5 with a shear-type attachment, shown in Fig. 12. The excavator had three links as shown in Fig. 12, which were the boom, the arm, and the attachment. Each of the actuators was driven by a hydraulic circuit of the structure illustrated in Fig. 2, with a single four-port spool valve acting as the collection of the four main control valves in Fig. 2. The control input u from the controller was interpreted as the spool position of the spool valve. The arm actuator involved the regenerative pipeline, while the boom actuator did not. The hydraulic circuits of the boom and arm actuators were interconnected through some pipelines, but during the experiments, the interconnecting pipelines were hardly in effect. Therefore, we regarded the circuits of the two actuators as independent from each other, each of them being driven by its own pump. Further detailed specifications and structures of the actuators are not provided in this paper due to proprietary restrictions.

The proposed controller was implemented to each of the boom and the arm actuators. The controller was constructed with MATLAB/Simulink and its sampling interval was set as $T = 0.01$ s. The controller was connected to the excavator over the Control Area Network (CAN). It commanded the opening ratios of the main control valves as the control input u through CAN and received the joint angles measured

by potentiometers. The measured angles were converted into the actuator length p , which were used as the inputs to the controller. The parameters of the proposed controller for the boom actuator were set as $K = 2.5 \times 10^5$ N/m, $B = 2.5 \times 10^2$ N·s/m, and $H = 0.5$ s, which are the same as Setting A_{bm} shown in Section V-B. The parameters for the arm actuator were set as $K = 1.5 \times 10^6$ N/m, $B = 2.0 \times 10^4$ N·s/m, and $H = 1.0$ s, which are the same as Setting B_{am}. Although the parameters were chosen based on the discussion in Section IV-B, we additionally tuned them in the experiments. As a result, the parameter values for the boom were chosen to be different from those that were most suited in the simulations in Section V-B.

The valve opening ratio u_{reg} of the regenerative pipeline of the arm actuator was manipulated by a built-in controller of the excavator, and its algorithm is proprietary. The proposed controller implemented to the arm actuator uses the value of u_{reg} as an input.

In the experiments, we did not test other controllers including the PID controller (42). As a practical matter, we needed to avoid risky trials with the 13-ton class excavator using controllers that have not been adequately validated in our environment.

B. Step Responses

Some experiments were performed to check the step responses with the proposed controller. In the experiments, the excavator was moved as illustrated in Fig. 13(a) to examine the step responses of the boom actuator, and also as in Fig. 14(a) for the arm actuator.

Fig. 13(b) shows the results of the boom actuator. As seen in the figure, the length p_{bm} of the boom actuator smoothly converged to the target length $p_{bm,d}$ in both boom-up and boom-down motions. Fig. 13(b) also shows that the control input u_{bm} was saturated for the first few seconds, but it did not result in overshoots or oscillations after that. These results illustrate the effect of the sliding-mode structure of the proposed controller.

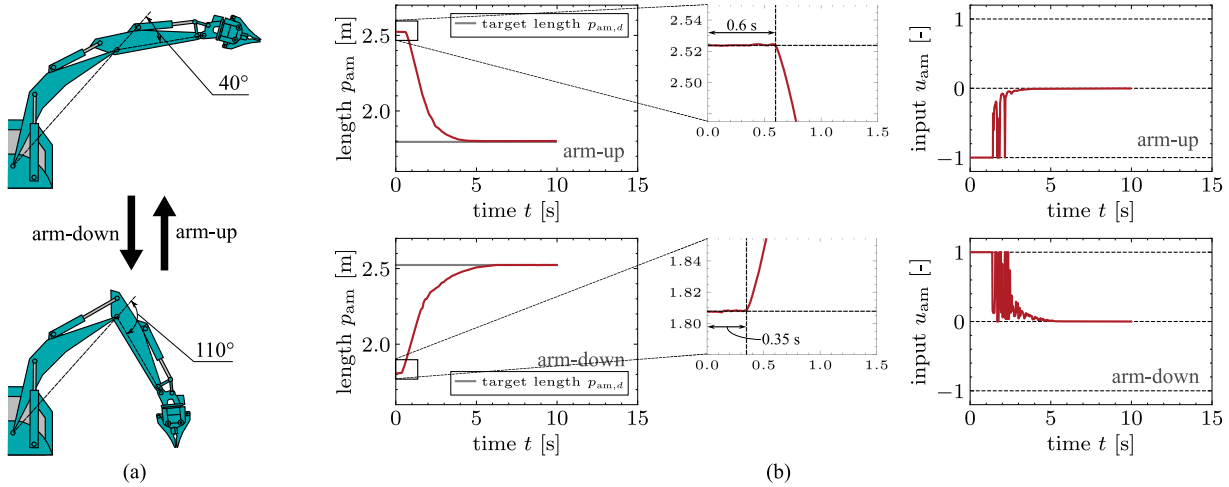


Fig. 14. Experiments of step responses of the arm actuators; (a) Configuration of the excavator and (b) step responses of the arm.

It should be noted that the employed parameter setting was not the same as the most suitable setting in the simulations in Section V-B, but resulted in no overshoots or oscillations in these experiments. The difference between the simulation and experiment results may be attributed to unmodeled factors of the excavator, such as joint frictions, the viscosity of the oil, and the compressibility of the oil.

Fig. 14(b) shows the results of the arm actuator. It shows similar features as those in Fig. 13(b), indicating that the controller properly worked also with the arm actuator. It shows some chattering-like behaviors in the control input u_{am} . It may be attributed to the imperfection of the regenerative-pipeline compensation, which can make the first argument of Θ_s in (26i) too small due to possible modeling errors. Such chattering in u_{am} would not be a practical issue because it does not result in physical vibration due to the dynamics of the spool valve and because it does not affect the convergence of the length p_{am} . Nevertheless, for improving the regenerative-pipeline compensation, it may be reasonable to employ a more accurate estimate of the external force \hat{g} in (25c), e.g., an estimated force based on the chamber pressures.

In the experiments with the arm actuator, we employed Setting B_{am}, which is the most suitable setting in the simulations in Section V-B. The experimental results were overall close to the simulation results with the same Setting B_{am} in Fig. 9(c), although there are more intense chattering-like behaviors in the control input u_{am} than the simulations.

The deadtime in the excavator was not accurately available, but it was estimated from the experimental results. From the zoomed graphs in Figs. 13(b) and 14(b), one can see that the time spent from the step input to the beginning of the motion was about 0.25 s and 0.15 s with the boom actuator, and 0.6 s and 0.35 s with the arm actuator, which can be seen as rough estimates of the deadtime. It should be noted that the proposed controller does not explicitly depend on the estimated deadtime, except that it may be used for the parameter tuning scheme discussed in Section IV-B. It should also be recalled that the controller parameters in the

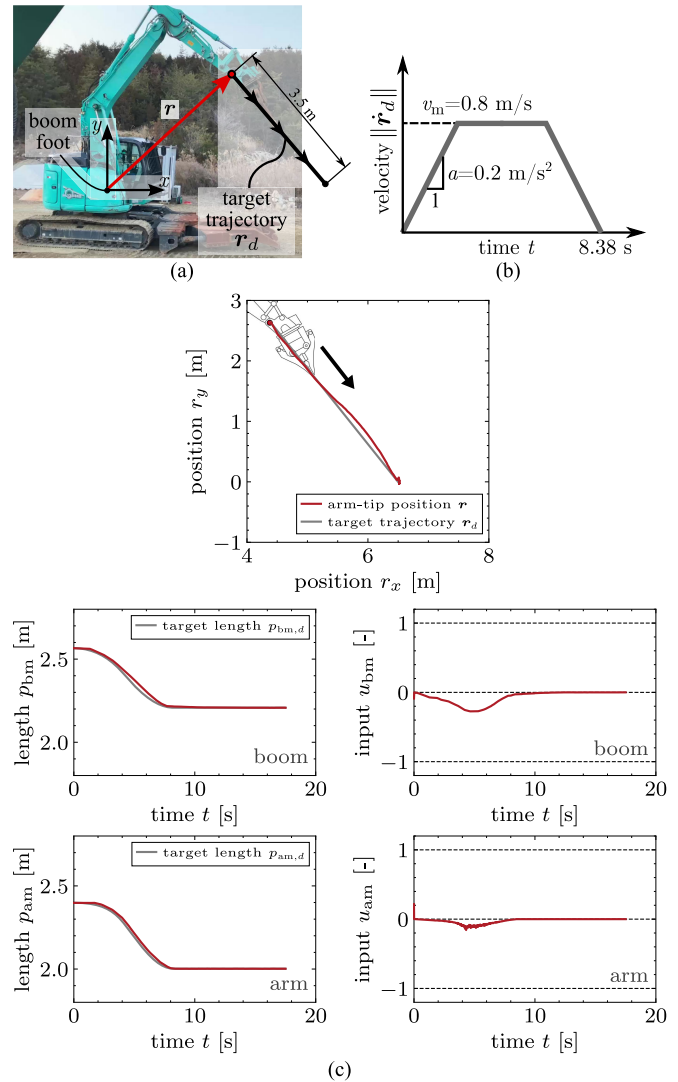


Fig. 15. Experiments of tracking along an oblique downward trajectory; (a) Target trajectory. (b) Velocity pattern. (c) Experimental results.

experiments were chosen by using the pole locations of the transfer function $G(s)$ in (38) with the estimated deadtime $T_d = 0.3$ s.

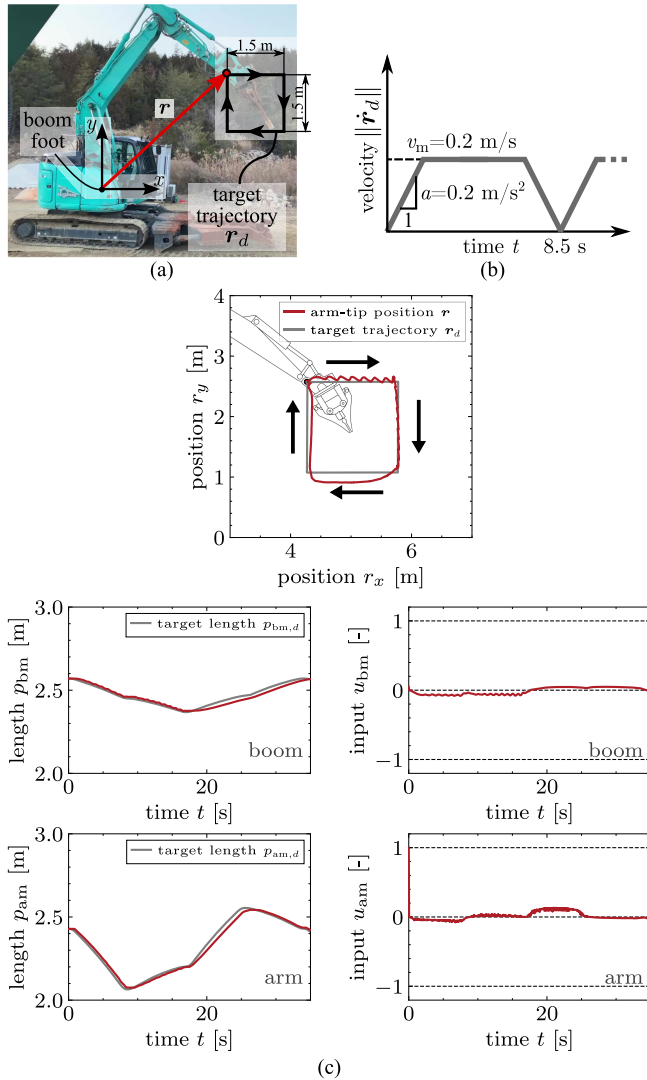


Fig. 16. Experiments of tracking along a square trajectory; (a) Target trajectory. (b) Velocity pattern. (c) Experimental results.

C. Trajectory-Tracking Control

We tested the proposed controller (15) with two trajectory-tracking tasks. The controller was implemented in each of the boom and arm actuators so that the arm-tip position \mathbf{r} should follow the target position \mathbf{r}_d . The target lengths $\{p_{bm,d}, p_{am,d}\}$ of the actuators were computed from the target arm-tip position \mathbf{r}_d through the inverse kinematics. The parameters were set the same as in the case of the step-response experiments in Section VI-B.

The first task was the tracking along a sloping-down trajectory shown in Fig. 15(a) with the trapezoidal pattern of the speed $\|\dot{\mathbf{r}}_d\|$ shown in Fig. 15(b). The results in Fig. 15(c) show that the tracking was properly achieved without oscillations or overshoots. Recall that the hydraulic actuators have a deadtime ranging from approximately 0.15 s to 0.6 s, as observed in the step responses shown in Figs. 13 and 14. For such actuators, the proposed controller, which does not explicitly compensate for the deadtime, achieved small positional errors and smooth convergence.

The second task was the tracking along a square-shaped trajectory shown in Fig. 16(a) with the trapezoidal speed pattern shown in Fig. 16(b). From the results in Fig. 16(c), one can see that the tracking was mostly successful with the excavator, which has the deadtime and the regenerative circuit. There were, however, some oscillations during the motions along the top and right edges ($t \in [0 \text{ s}, 18 \text{ s}]$) of the trajectory, which coincided with the boom-down motion. The oscillations are visible in the graphs of the position \mathbf{r} , although it is not very visible in the graphs of the actuator lengths $\{p_{bm}, p_{am}\}$. The oscillations can be seen as a stick-slip-like phenomenon, which is presumably caused by the dead zone in the control valves and the joint friction. In fact, a careful examination of Fig. 16(c) revealed that the length p_{bm} started to move only when the control input u_{bm} was below -0.1 . In addition, there were also some positional errors about 0.1 m during the motions along the bottom and left edges ($t \in [18 \text{ s}, 26 \text{ s}]$) of the trajectory. It may be attributed to the inaccuracy of the actuator model in the controller.

The oscillation and positional error may be suppressed by improving the actuator model in the controller, e.g., by including the dead zone of the control valves. In addition, the oil flowrate from the pump, which was treated as a constant in the present controller, may need to be substituted by measured values from an appropriate sensor.

VII. CONCLUSION

This paper has proposed a position controller for hydraulic actuators with deadtime and regenerative pipelines. The controller is constructed by combining three components, which are a PD controller, a sliding mode controller, and a previously-proposed quasistatic actuator model, in a particular differential-algebraic manner. By employing the actuator model, the proposed controller accounts for the saturations of the actuator force. In addition, due to the use of the PD controller, it realizes a certain level of robustness against the presence of the deadtime. Furthermore, the controller has been extended to deal with regenerative pipelines in the hydraulic actuators. We also have provided some analyses that can be used for tuning the controller parameters. The proposed controller has been validated with simulations and experiments employing a 13-ton class excavator, which has deadtime of 0.1 s to 0.6 s and a regenerative pipeline in the arm actuator. In the simulations and experiments, it has been shown that some different tasks, including set-point control tasks and trajectory-tracking tasks, can be achieved with a single common set of parameter settings.

Future work should address combining the controller with disturbance compensation techniques, probably based on the sensor information of the pressures and flowrates in the actuators and the circuits. It would enhance the accuracy of the controller, especially when the excavator is loaded. In addition, one should also consider the fact that, in commercial excavators, the structures of hydraulic circuits may be more involved than that has been considered in this paper; for example, a single pump may drive multiple actuators. The extension of the controller to deal with such complicated circuit structures should also be sought.

APPENDIX PROOF OF THEOREM 1

Proof of Theorem 1: Let us define $v_e \triangleq v - \dot{p}_d$ and $\phi \triangleq g - \hat{g} - M\ddot{p}_d$. Then, the system (30) can be rewritten as follows:

$$\dot{\mathbf{x}} = \mathbf{A}(\beta)\mathbf{x} - \mathbf{b}(\beta) \text{dzn}_{\Gamma_s(1/B, \mathbf{g}^T \mathbf{x} + \hat{g}/B + \dot{p}_d, B)}(\mathbf{c}^T \mathbf{x} - \hat{g}) + \mathbf{d}\phi \quad (43)$$

where

$$\mathbf{x} \triangleq [\sigma, v_e, e]^T \quad (44)$$

$$\mathbf{A}(\beta) \triangleq \begin{bmatrix} -(B + \beta)/M & 1 & HK/M \\ -(B + \beta)/(HM) & 0 & K/M \\ -1/H & 0 & 0 \end{bmatrix} \quad (45)$$

$$\mathbf{d} \triangleq [H/M, 1/M, 0]^T \quad (46)$$

$$\mathbf{b}(\beta) \triangleq [H(B + \beta)/(BM), (B + \beta)/(BM), 1/B]^T \quad (47)$$

$$\mathbf{c} \triangleq [-B/H, 0, K]^T \quad (48)$$

$$\mathbf{g} \triangleq [0, 1, -K/B]^T \quad (49)$$

$$\text{dzn}_{\mathcal{X}}(f) \triangleq f - \text{sat}_{\mathcal{X}}(f). \quad (50)$$

Here, we can use the following property of the function dzn

$$\text{dzn}_{\mathcal{X}}(x - a) = \text{dzn}_{\mathcal{X}+a}(x). \quad (51)$$

Then, we can rewrite (43) as follows:

$$\dot{\mathbf{x}} = \mathbf{A}(\beta)\mathbf{x} - \mathbf{b}(\beta) \text{dzn}_{\mathcal{F}(\mathbf{g}^T \mathbf{x}, B)}(\mathbf{c}^T \mathbf{x}) + \mathbf{d}\phi \quad (52)$$

where

$$\mathcal{F}(v, u) \triangleq \Gamma_s(1/B, v + \dot{p}_d + \hat{g}/B, u) + \hat{g}. \quad (53)$$

It can be shown that $\mathbf{A}(\beta)$ is Hurwitz for all $\beta \geq 0$ if (32a) is satisfied. Therefore, for any diagonal and positive definite matrix $\mathbf{Q} \succ 0$, there exists a symmetric and positive definite matrix $\mathbf{P}(\beta) \succ 0$ with which

$$\mathbf{Q} = -(\mathbf{P}(\beta)\mathbf{A}(\beta) + \mathbf{A}(\beta)^T \mathbf{P}(\beta))/2 \quad (54)$$

is satisfied. With such a matrix $\mathbf{P}(\beta)$, let us define $V \triangleq \mathbf{x}^T \mathbf{P}(\beta) \mathbf{x}/2$. Then, we have

$$\begin{aligned} \dot{V} &= -\mathbf{x}^T \mathbf{Q} \mathbf{x} - \mathbf{x}^T \mathbf{P}(\beta) \mathbf{b}(\beta) \text{dzn}_{\mathcal{F}(\mathbf{g}^T \mathbf{x}, B)}(\mathbf{c}^T \mathbf{x}) \\ &\quad + \mathbf{x}^T \mathbf{P}(\beta) \mathbf{d} \phi + \mathbf{x}^T \mathbf{R}(\beta) \mathbf{x} \dot{\beta} \\ &\leq -(\lambda_Q - \gamma_R(\beta)|\dot{\beta}|)\|\mathbf{x}\|^2 + \alpha \|\mathbf{P}(\beta) \mathbf{d}\| \|\mathbf{x}\| \\ &\quad + \|\mathbf{P}(\beta) \mathbf{b}(\beta)\| \|\mathbf{x}\| |\text{dzn}_{\mathcal{F}(\mathbf{g}^T \mathbf{x}, B)}(\mathbf{c}^T \mathbf{x})| \end{aligned} \quad (55)$$

where

$$\mathbf{R}(\beta) \triangleq \frac{1}{2} \frac{\partial \mathbf{P}(\beta)}{\partial \beta}. \quad (56)$$

Here, λ_Q is the minimum eigenvalue of \mathbf{Q} and $\gamma_R(\beta)$ is the maximum absolute value of the eigenvalues of $\mathbf{R}(\beta)$.

The matrix $\mathbf{P}(\beta)$ can be analytically obtained (by using, e.g., `LyapunovSolve` function of Mathematica) as a rational function of β . From the analytical representation of $\mathbf{P}(\beta)$, it can be seen that $\|\mathbf{P}(\beta) \mathbf{b}(\beta)\|$ and $\|\mathbf{P}(\beta) \mathbf{d}\|$ are bounded if (32a) is satisfied. It can also be seen that all the elements of $\mathbf{R}(\beta)$ are bounded, and thus $\gamma_R(\beta)$ is also bounded.

Now, let us focus on the third term of the right-hand side of (55). With some straightforward derivations, the following can be seen:

$$\begin{aligned} |\text{dzn}_{\mathcal{F}(v, B)}(f)| &= \max(0, f - \mathcal{F}(v, 1)) \\ &\quad + \max(0, -f + \mathcal{F}(v, -1)). \end{aligned} \quad (57)$$

From the property of Γ_s , one can see that

$$-B \leq \frac{\partial \mathcal{F}(v, u)}{\partial v} \leq 0, \quad (58)$$

and thus the following is satisfied:

$$0 \leq v(\mathcal{F}(0, u) - \mathcal{F}(v, u)) \leq Bv^2. \quad (59)$$

It is equivalent to

$$\mathcal{F}(0, u) - B \max(v, 0) \leq \mathcal{F}(v, u) \leq \mathcal{F}(0, u) - B \min(v, 0), \quad (60)$$

which implies the following:

$$\mathcal{F}(0, u) - B|v| \leq \mathcal{F}(v, u) \leq \mathcal{F}(0, u) + B|v|. \quad (61)$$

By using (61), one can see that the terms of the right-hand side of (57) are upperbounded as follows:

$$\begin{aligned} \max(0, f - \mathcal{F}(v, 1)) &\leq \max(0, f - \mathcal{F}(0, 1) + B|v|) \\ &\leq \max(0, |f| + B|v| - \delta) \end{aligned} \quad (62)$$

$$\begin{aligned} \max(0, -f + \mathcal{F}(v, -1)) &\leq \max(0, -f + \mathcal{F}(0, -1) + B|v|) \\ &\leq \max(0, |f| + B|v| - \delta). \end{aligned} \quad (63)$$

Here, we used the fact that $\mathcal{F}(0, -1) \leq -\delta$ and $\delta \leq \mathcal{F}(0, 1)$ derived from the condition (32b). Noting that the two terms of the right-hand side of (57) cannot be non-zero simultaneously, we have the following:

$$|\text{dzn}_{\mathcal{F}(v, B)}(f)| \leq \max(0, |f| + B|v| - \delta). \quad (64)$$

By using (64) in (55), an upperbound of \dot{V} can be given as follows:

$$\begin{aligned} \dot{V} &\leq -(\lambda_Q - \gamma_R(\beta)|\dot{\beta}|)\|\mathbf{x}\|^2 + \alpha \|\mathbf{P}(\beta) \mathbf{d}\| \|\mathbf{x}\| \\ &\quad + \|\mathbf{P}(\beta) \mathbf{b}(\beta)\| \|\mathbf{x}\| \max(0, \|\mathbf{c}\| \|\mathbf{x}\| + B\|\mathbf{g}\| \|\mathbf{x}\| - \delta) \\ &\leq -c_0 \|\mathbf{x}\| (\min(\|\mathbf{x}\|, -c_1 \|\mathbf{x}\| + c_2) - \alpha c_3) \end{aligned} \quad (65)$$

where

$$c_0 \triangleq \lambda_Q - \overline{\gamma_R(\beta)} |\dot{\beta}| \quad (66)$$

$$c_1 \triangleq \frac{\|\mathbf{P}(\beta) \mathbf{b}(\beta)\| (\|\mathbf{c}\| + B\|\mathbf{g}\|)}{c_0} - 1 \quad (67)$$

$$c_2 \triangleq \delta \frac{\|\mathbf{P}(\beta) \mathbf{b}(\beta)\|}{c_0} \quad (68)$$

$$c_3 \triangleq \frac{\|\mathbf{P}(\beta) \mathbf{d}\|}{c_0}. \quad (69)$$

Here, $\overline{\gamma_R(\beta)}$, $\overline{\|\mathbf{P}(\beta) \mathbf{b}(\beta)\|}$, and $\overline{\|\mathbf{P}(\beta) \mathbf{d}\|}$ are upperbounds of $\gamma_R(\beta)$, $\|\mathbf{P}(\beta) \mathbf{b}(\beta)\|$, and $\|\mathbf{P}(\beta) \mathbf{d}\|$, respectively. Therefore, $\dot{V} < 0$ is satisfied when $c_0 > 0$ and

$$\min(\|\mathbf{x}\|, -c_1 \|\mathbf{x}\| + c_2) > \alpha c_3 \quad (70)$$

are satisfied. Here, (70) is equivalent to

$$\alpha c_3 < \|\mathbf{x}\| < \begin{cases} (c_2 - \alpha c_3)/c_1 & \text{if } c_1 > 0 \\ \infty & \text{otherwise.} \end{cases} \quad (71)$$

For the existence of \mathbf{x} satisfying (71), when $c_1 > 0$, α must satisfy the following:

$$\alpha < \frac{c_2}{c_3(c_1 + 1)} = \frac{\delta(\lambda_Q - \overline{\gamma_R(\beta)}|\dot{\beta}|)}{\|\mathbf{P}(\beta)\mathbf{d}\|(\|\mathbf{c}\| + B\|\mathbf{g}\|)}. \quad (72)$$

Therefore, if $|\dot{\beta}|$ is small enough to satisfy $|\dot{\beta}| < \lambda_Q/\overline{\gamma_R(\beta)}$ and if α is small enough to satisfy (72), one can say that the state \mathbf{x} is uniformly ultimately bounded with the ultimate bound $\alpha c_3 B$, which is a neighborhood of the origin.

In addition, if $\alpha = 0$, i.e., if $\phi \equiv 0$ and $\ddot{p}_d \equiv 0$, $\dot{V} < 0$ is satisfied in $\mathbf{x} \in (c_2/c_1)B$ if $c_1 < 0$ and globally otherwise. This means that the origin is asymptotically stable if $\phi \equiv 0$ and $\ddot{p}_d \equiv 0$.

REFERENCES

- [1] J. Kim, M. Jin, W. Choi, and J. Lee, "Discrete time delay control for hydraulic excavator motion control with terminal sliding mode control," *Mechatronics*, vol. 60, pp. 15–25, Jun. 2019, doi: [10.1016/j.mechatronics.2019.04.008](https://doi.org/10.1016/j.mechatronics.2019.04.008).
- [2] P. H. Chang and S.-J. Lee, "A straight-line motion tracking control of hydraulic excavator system," *Mechatronics*, vol. 12, no. 1, pp. 119–138, Feb. 2002, doi: [10.1016/S0957-4158\(01\)00014-9](https://doi.org/10.1016/S0957-4158(01)00014-9).
- [3] Y. Wang, L. Gu, B. Chen, and H. Wu, "A new discrete time delay control of hydraulic manipulators," *Proc. Inst. Mech. Eng., I, J. Syst. Control Eng.*, vol. 231, no. 3, pp. 168–177, Mar. 2017, doi: [10.1177/0959651816689340](https://doi.org/10.1177/0959651816689340).
- [4] S. Kim, J. Park, S. Kang, P. Y. Kim, and H. J. Kim, "A robust control approach for hydraulic excavators using μ -synthesis," *Int. J. Control, Autom. Syst.*, vol. 16, no. 4, pp. 1615–1628, Aug. 2018, doi: [10.1007/s12555-017-0071-9](https://doi.org/10.1007/s12555-017-0071-9).
- [5] Y. Ye, C.-B. Yin, Y. Gong, and J.-J. Zhou, "Position control of nonlinear hydraulic system using an improved PSO based PID controller," *Mech. Syst. Signal Process.*, vol. 83, pp. 241–259, Jan. 2017, doi: [10.1016/j.ymsp.2016.06.010](https://doi.org/10.1016/j.ymsp.2016.06.010).
- [6] H. Feng, W. Ma, C. Yin, and D. Cao, "Trajectory control of electro-hydraulic position servo system using improved PSO-PID controller," *Autom. Construction*, vol. 127, Jul. 2021, Art. no. 103722, doi: [10.1016/j.autcon.2021.103722](https://doi.org/10.1016/j.autcon.2021.103722).
- [7] H. Feng et al., "Robotic excavator trajectory control using an improved GA based PID controller," *Mech. Syst. Signal Process.*, vol. 105, pp. 153–168, May 2018, doi: [10.1016/j.ymsp.2017.12.014](https://doi.org/10.1016/j.ymsp.2017.12.014).
- [8] H. Feng, C. Yin, W. Ma, H. Yu, and D. Cao, "Parameters identification and trajectory control for a hydraulic system," *ISA Trans.*, vol. 92, pp. 228–240, Sep. 2019, doi: [10.1016/j.isatra.2019.02.022](https://doi.org/10.1016/j.isatra.2019.02.022).
- [9] Y. Li and Q. Wang, "Adaptive neural finite-time trajectory tracking control of hydraulic excavators," *Proc. Inst. Mech. Eng., I, J. Syst. Control Eng.*, vol. 232, no. 7, pp. 909–925, Aug. 2018, doi: [10.1177/0959651818767770](https://doi.org/10.1177/0959651818767770).
- [10] J. Park, B. Lee, S. Kang, P. Y. Kim, and H. J. Kim, "Online learning control of hydraulic excavators based on echo-state networks," *IEEE Trans. Autom. Sci. Eng.*, vol. 14, no. 1, pp. 249–259, Jan. 2017, doi: [10.1109/TASE.2016.2582213](https://doi.org/10.1109/TASE.2016.2582213).
- [11] M. Lee, H. Choi, C. Kim, J. Moon, D. Kim, and D. Lee, "Precision motion control of robotized industrial hydraulic excavators via data-driven model inversion," *IEEE Robot. Autom. Lett.*, vol. 7, no. 2, pp. 1912–1919, Apr. 2022, doi: [10.1109/LRA.2022.3142389](https://doi.org/10.1109/LRA.2022.3142389).
- [12] P. Egli and M. Hutter, "A general approach for the automation of hydraulic excavator arms using reinforcement learning," *IEEE Robot. Autom. Lett.*, vol. 7, no. 2, pp. 5679–5686, Apr. 2022, doi: [10.1109/LRA.2022.3152865](https://doi.org/10.1109/LRA.2022.3152865).
- [13] H. Feng et al., "A new adaptive sliding mode controller based on the RBF neural network for an electro-hydraulic servo system," *ISA Trans.*, vol. 129, pp. 472–484, Oct. 2022, doi: [10.1016/j.isatra.2021.12.044](https://doi.org/10.1016/j.isatra.2021.12.044).
- [14] Y. Yamamoto et al., "A sliding-mode set-point position controller for hydraulic excavators," *IEEE Access*, vol. 9, pp. 153735–153749, 2021, doi: [10.1109/ACCESS.2021.3128215](https://doi.org/10.1109/ACCESS.2021.3128215).
- [15] R. Kikuuwe, T. Okada, H. Yoshihara, T. Doi, T. Nanjo, and K. Yamashita, "A nonsmooth quasi-static modeling approach for hydraulic actuators," *J. Dyn. Syst., Meas., Control*, vol. 143, no. 12, Dec. 2021, Art. no. 121002, doi: [10.1115/1.4051894](https://doi.org/10.1115/1.4051894).
- [16] J. E. Normey-Rico and E. F. Camacho, *Control Dead-Time Processes*. Cham, Switzerland: Springer, 2007.
- [17] M. H. Nguyen, H. V. Dao, and K. K. Ahn, "Extended sliding mode observer-based high-accuracy motion control for uncertain electro-hydraulic systems," *Int. J. Robust Nonlinear Control*, vol. 33, no. 2, pp. 1351–1370, Jan. 2023, doi: [10.1002/rnc.6421](https://doi.org/10.1002/rnc.6421).
- [18] J. Xu and H.-S. Yoon, "Sliding mode control of hydraulic excavator for automated grading operation," *SAE Int. J. Commercial Vehicles*, vol. 11, no. 2, pp. 113–124, Jun. 2018, doi: [10.4271/02-11-02-0010](https://doi.org/10.4271/02-11-02-0010).
- [19] R. Kikuuwe, S. Yasukouchi, H. Fujimoto, and M. Yamamoto, "Proxy-based sliding mode control: A safer extension of PID position control," *IEEE Trans. Robot.*, vol. 26, no. 4, pp. 670–683, Aug. 2010, doi: [10.1109/TRO.2010.2051188](https://doi.org/10.1109/TRO.2010.2051188).
- [20] R. Kikuuwe, "A sliding-mode-like position controller for admittance control with bounded actuator force," *IEEE/ASME Trans. Mechatronics*, vol. 19, no. 5, pp. 1489–1500, Oct. 2014, doi: [10.1109/TMECH.2013.2286411](https://doi.org/10.1109/TMECH.2013.2286411).
- [21] W. Borutzky, B. Barnard, and J. Thoma, "An orifice flow model for laminar and turbulent conditions," *Simul. Model. Pract. Theory*, vol. 10, nos. 3–4, pp. 141–152, Nov. 2002, doi: [10.1016/S1569-190X\(02\)00092-8](https://doi.org/10.1016/S1569-190X(02)00092-8).
- [22] K. Kim, M. Kim, D. Kim, and D. Lee, "Modeling and velocity-field control of autonomous excavator with main control valve," *Automatica*, vol. 104, pp. 67–81, Jun. 2019, doi: [10.1016/j.automatica.2019.02.041](https://doi.org/10.1016/j.automatica.2019.02.041).
- [23] D. Cristofori and A. Vacca, "Modeling hydraulic actuator mechanical dynamics from pressure measured at control valve ports," *Proc. Inst. Mech. Eng., I, J. Syst. Control Eng.*, vol. 229, no. 6, pp. 541–558, Jul. 2015, doi: [10.1177/0959651814568366](https://doi.org/10.1177/0959651814568366).
- [24] A. Lichtarowicz, R. K. Duggins, and E. Markland, "Discharge coefficients for incompressible non-cavitating flow through long orifices," *J. Mech. Eng. Sci.*, vol. 7, no. 2, pp. 210–219, Jun. 1965, doi: [10.1243/jmes_jour_1965_007_029_02](https://doi.org/10.1243/jmes_jour_1965_007_029_02).
- [25] Y. Ye, C.-B. Yin, X.-D. Li, W.-J. Zhou, and F.-F. Yuan, "Effects of groove shape of notch on the flow characteristics of spool valve," *Energy Convers. Manage.*, vol. 86, pp. 1091–1101, Oct. 2014, doi: [10.1016/j.enconman.2014.06.081](https://doi.org/10.1016/j.enconman.2014.06.081).
- [26] D. Wu, R. Burton, and G. Schoenau, "An empirical discharge coefficient model for orifice flow," *Int. J. Fluid Power*, vol. 3, no. 3, pp. 13–19, Jan. 2002, doi: [10.1080/14399776.2002.10781143](https://doi.org/10.1080/14399776.2002.10781143).
- [27] R. Kikuuwe, Y. Yamamoto, and B. Brogliato, "Implicit implementation of nonsmooth controllers to nonsmooth actuators," *IEEE Trans. Autom. Control*, vol. 67, no. 9, pp. 4645–4657, Sep. 2022, doi: [10.1109/TAC.2022.3163124](https://doi.org/10.1109/TAC.2022.3163124).
- [28] H. K. Khalil, *Nonlinear Systems*, 3rd ed. Upper Saddle River, NJ, USA: Prentice-Hall, 2002.
- [29] R. Kikuuwe, N. Takesue, A. Sano, H. Mochiyama, and H. Fujimoto, "Admittance and impedance representations of friction based on implicit Euler integration," *IEEE Trans. Robot.*, vol. 22, no. 6, pp. 1176–1188, Dec. 2006, doi: [10.1109/TRO.2006.886262](https://doi.org/10.1109/TRO.2006.886262).
- [30] R. Kikuuwe, T. Okada, H. Yoshihara, T. Doi, T. Nanjo, and K. Yamashita, "Nonsmooth quasistatic modeling of hydraulic actuators," 2021, *arXiv:2102.11381*.



Yuki Yamamoto received the B.E. and M.E. degrees in mechanical engineering from Hiroshima University, Hiroshima, Japan, in 2020 and 2022, respectively, where he is currently pursuing the Ph.D. degree with the Graduate School of Advanced Science and Engineering (Mechanical Engineering Program). He is also a Research Fellow with the Japan Society for the Promotion of Science. His research interests include control engineering, dynamics identification, mechatronics, and force estimation of hydraulic actuators.



Jinjun Qiu received the M.E. and Ph.D. degrees from Kyushu University, Fukuoka, Japan, in 2009 and 2012, respectively.

In 2018, he joined Kobelco Construction Machinery Company Ltd., Hiroshima, Japan. At the time of writing, he was a member with the Automated System Engineering Group, Advanced Technology Engineering Department, Kobelco Construction Machinery Company Ltd.



Koji Yamashita received the M.Eng. degree in electrical engineering from the Toyohashi University of Technology, Japan, in 1994.

From 1994 to 1999, he was with Kobe Steel, Ltd. In 1999, he joined Kobelco Construction Machinery Company Ltd., Hiroshima, Japan. Since 2020, he has been a Visiting Professor with Hiroshima University, Japan. He is currently the General Manager of the Product Development Engineering Department, Kobelco Construction Machinery Company Ltd.



Takayuki Doi joined Kobelco Construction Machinery Company Ltd., Hiroshima, Japan, in 2006. He is currently the Group Leader of the Technical Support Group, Hiroshima, and the Business Development Department, Kobelco Construction Machinery Company Ltd. He is engaged in the development of hydraulic excavators' electricity/control systems.



Takao Nanjo received the M.E. degree in mechanical engineering from Kyushu University, Fukuoka, Japan, in 1992.

From 1992 to 2017, he was with Kobe Steel, Ltd. In 2017, he joined Kobelco Construction Machinery Company Ltd., Hiroshima, Japan, where he is currently the Senior Manager of the Strategic Research and Development Group, Advanced Technology Engineering Department.

Mr. Nanjo is a member of the Japan Society of Mechanical Engineers.



Ryo Kikuuwe (Member, IEEE) received the B.S., M.S., and Ph.D. (Eng.) degrees in mechanical engineering from Kyoto University, Kyoto, Japan, in 1998, 2000, and 2003, respectively.

From 2003 to 2007, he was an Endowed-Chair Research Associate with the Nagoya Institute of Technology, Nagoya, Japan. From 2007 to 2017, he was an Associate Professor with the Department of Mechanical Engineering, Kyushu University, Fukuoka, Japan. From 2014 to 2015, he was a Visiting Researcher with Inria Grenoble Rhône-

Alpes, Saint-Ismier, France. He is currently a Full Professor with the Graduate School of Advanced Science and Engineering, Hiroshima University, Hiroshima, Japan. His research interests include force control of robot manipulators, real-time simulation for physics-based animation, and engineering applications of differential inclusions.

Prof. Kikuuwe is a member of the Robotics Society of Japan, the Japan Society of Mechanical Engineers, the Society of Instrument and Control Engineers (Japan), and the Virtual Reality Society of Japan. He was a recipient of the Best Paper Award of Advanced Robotics in 2013 and the Young Investigator Excellence Award from the Robotics Society of Japan in 2005.